# Experimental cross sections for water ionization due to the impact of light ions-A review

Mario Bernal, Jacinto Liendo, Sebastien Incerti, Ziad Francis, Hoang Tran

# Experimental cross sections for water ionization due to the impact of light ions. A review.

**Mario A. Bernal**

Instituto de Física Gleb Wataghin. Universidade Estadual de Campinas, SP. Brazil

E-mail: mbernalrod@gmail.com

**Jacinto A. Liendo**

Departamento de Física. Universidad Simón Bolívar. Caracas, Venezuela

**Sebastien Incerti**

Univ. Bordeaux, CNRS, CENBG, UMR 5797, F-33170 Gradignan, France

**Ziad Francis**

Saint Joseph University, U.R. Mathématiques et Modélisation, Beirut, Lebanon

**Hoang N. Tran**

Univ. Bordeaux, CNRS, CENBG, UMR 5797, F-33170 Gradignan, France

**Abstract.** This work is a short review on the experimental cross sections for water ionization due to the impact of light ions ($Z \leq 6$), including related processes such as electron capture and water molecule fragmentation. These cross sections are crucial in studies dealing with the biological effects produced by the impact of ions on living beings. Physical interpretations of the experimental results are also provided.

PACS numbers: 34.50.Gb

*Keywords*: water ionization, ion beams, protons, alpha particles, cross sections, water fragmentation

Submitted to:

## 1. Introduction

The ionization problem is of great importance in areas such as medical radiation physics, plasma physics, space physics, and other areas. This process is included in virtually all the Monte Carlo codes used to simulate the radiation-matter interaction. Specific areas, such as nanodosimetry and computational radiobiology require knowledge of liquid water target ionization cross sections but setting up experiments with this aggregation state has been very difficult so far. Experiments for the determination of ionization cross sections due to the impact of ions on water are very scarce and all of them have used water vapor as a target. Up to our knowledge, no experimental determination of ionization cross sections has been carried out in liquid water, mainly due to the difficulty to set up a liquid target and the fact that electrons produced during ionizations can be absorbed within this target with a relatively high probability. In this work, only non-relativistic light ions (Z$\leq$6) are considered.

Atomic units are used throughout this review, unless otherwise stated. In this system, the mass is expressed in units of the electron rest mass $m$; the length, in units of the Bohr radius $a_o = \hbar^2/(me^2)$; the energy, in units of Hartrees ($1H = me^4/\hbar^2$=2 Ry=27.2 eV); the momentum, in units of $\hbar/a_o = me^2/\hbar$; and the speed, in units of $e^2/\hbar$. In addition, $e = m = \hbar = 1$.

**The ionization problem**

When a charged particle interacts with an atom or molecule, it can remove electrons from those targets, leaving them ionized. Electronic excitation of these targets can be also observed during such collisions. This interaction is mediated by a potential with two components: the Coulomb and the magnetic ones. The electrostatic potential originates from the charges of the projectile and the target electron, whilst the magnetic potential comes from the interaction between the magnetic field induced by the projectile current and the target electron spin. The magnetic component is only important for relativistic projectiles, which are out of the scope of this review, where energies up to about a few ten MeV/u are taken into account. Several charge-transfer processes can occur in this situation. Atomic electrons can be removed and set in motion, which is known as direct ionization, they can be captured by the projectile into a bound state or the projectile can lose its own electrons, if it is not a bare ion. These processes are represented in reactions (1-3), where $n$ is the number of electrons transferred in the collision. Processes with $n > 1$, are known as multiple ionization, multiple electron capture, or multiple electron loss, respectively, and they are important only for relatively heavy ions.

$$A^{z+} + H_2O \rightarrow H_2O^{n+} + A^{z+} + ne^-(direct\ ionization) \quad (1)$$

$$A^{z+} + H_2O \rightarrow H_2O^{n+} + A^{(z-n)+}(electron\ capture) \quad (2)$$

$$A^{z+} + H_2O \rightarrow H_2O + A^{(z+n)+} + ne^-(electron\ loss) \quad (3)$$

Charge-transfer processes are part of the ionization problem. Charged heavy particles can capture one or more electrons from the target molecule, leaving this target

ionized. This is the case of the electron capture by protons and alpha particles. The latter are also capable of capturing up to two electrons at once. Electron capture cross section maximizes when the projectile travels at the orbital electron speed. It could be seen as a resonant process. Of course, the water molecule has four orbitals with energies along a short range, going from about 11 eV up to 32 eV. Therefore, it is expected to observe a wide plateau in the cross section as a function of the projectile energy or speed. Captures from the Oxygen K-shell, with binding energy of ∼540 eV, is much less probable.

Since ions can lose or gain charge (electrons) there is an expected value for the projectile charge which depends on the projectile energy. This dependence can be explained by the balance between electron capture and loss cross sections, which depend on the projectile energy. For relatively low energies, at which the projectile speed gets closer to that of the orbital electron, electron capture is more probable than electron loss, so projectiles tend to have lower charges, and vice-versa. As the energy of dressed projectile increases, the probability for them to be liberated of their electrons during collisions with target molecules also increases. Thus, as the energy increases, the expected charge value increases.

**Theoretical ionization cross sections**

The importance of ionization among other competitive processes can be quantified by the corresponding cross section. For an ion, that travels along a virtually straight trajectory, the ionization cross section can be written using the impact-parameter approximation [1]

$$\frac{d^3\sigma}{d\mathbf{k}} = \int d\rho \, |a_{if}(\rho)|^2 \,, \tag{4}$$

where $a_{if}(\rho)$ is the transition amplitude from the initial $i$ and final $f$ states of the target electron, $\mathbf{k}$ is the electron momentum, and $\rho$ is the two-dimensional impact parameter vector. These two dimensions can be seen as the polar coordinates of the projectile in the plane normal to the incidence with the origin at the target. For determining the transition amplitude ($a_{if}(\rho)$), it is necessary to know the initial and final electronic wave functions, which poses the main hurdle when dealing with theoretical ionization cross sections.

Knowing that the volume element in the momentum space is $d\mathbf{k} = k^2 dk d\Omega$, the double differential cross section (DDCS) can be expressed as

$$\sigma(W,\theta) = \frac{d^2\sigma}{dW d\Omega} = k \int d\rho \, |a_{if}(\rho)|^2 \,, \tag{5}$$

with $d\Omega$ and $W = \frac{1}{2}k^2$ being the emitted electron differential solid angle and asymptotic kinetic energy, respectively. This cross section represents the probability, commonly expressed in $cm^2/(eV\,sr)$, that the electron is emitted along the direction $(\Omega, \Omega + d\Omega)$ and with an energy $(W, W + dW)$. It is also known as the angular distribution for electrons emitted at a given energy. For a problem with cylindrical symmetry, the

DDCS is determined by the polar angle $\theta$, which can be a fair approximation based on the fact that water molecules are randomly oriented in space.

If the DDCS is integrated over solid angle or electron energy, the following single differential cross sections (SDCS) are obtained

$$\sigma(W) = \frac{d\sigma}{dW} = \int d\Omega \sigma(W, \theta), \tag{6}$$

$$\sigma(\theta) = \frac{d\sigma}{d\Omega} = \int dW \sigma(W, \theta). \tag{7}$$

Integration of the SDCS leads to the total cross section

$$\sigma = \int dW \sigma(W) = \int d\Omega \sigma(\theta). \tag{8}$$

The stopping cross section (SCS) quantifies the capacity of a medium to slow down charged particles. The portion of this quantity associated to the ionization of the medium is defined as

$$SCS_{ion} = \int E\sigma(E)dE, \tag{9}$$

where E=W+I, with I being the electron binding energy. The stopping power (S) [2] can be calculated as $S = N \times SCS$, where $N$ is the number of targets, atoms or molecules, per unit volume.

**Main features of ionization cross sections**

For relatively high projectile speeds, the first Born (B1) approximation is commonly used for determining the transition amplitude defined in eq. (4). This is a first order perturbative approximation in which the whole interaction potential is used as perturbation. Then the transition amplitude in the impact parameter approximation, for a heavy charged particle traveling along the $z$ axis, can be written as [3]

$$a_{if}^{B1}(\rho) = -\frac{i}{v_p} \int_{-\infty}^{+\infty} dz e^{iqz} \Big\langle \Psi_f(\mathbf{r}) \Big| \frac{-Z_p}{|\mathbf{R} - \mathbf{r}|} \Big| \Psi_i(\mathbf{r}) \Big\rangle, \tag{10}$$

where $\Psi_i(\mathbf{r})$ and $\Psi_f(\mathbf{r})$ are the initial and final electronic wave functions, $Z_p$ and $v_p$ are the projectile charge and speed, respectively, $q$ is the momentum transfer, and $\mathbf{R}$ and $\mathbf{r}$ are the positions of the projectile and atomic electron, respectively. The reader should notice that, since the transition amplitude enters in eq. (5)as squared, then the corresponding cross section will be proportional to $(Z_p/v_p)^2$.

The higher the projectile charge, the stronger the perturbation and the lower the accuracy of this approximation. Strong perturbations can be also observed at low projectile speeds. For protons, this approximation provides acceptable accuracy for energies above ∼200 keV. Another important consequence of this approximation is that the influence of the projectile on the electronic wave function at the exit channel, after the ionization, is eliminated. This means that only the influence of the target atom on the emitted electron is taken into account, the so-call one-center effects. Thus, the only structure observed in the angular distribution of emitted electrons is the so-called binary peak. This peak appears at the polar angle along which the electron would be

ejected during a classical binary collision with the projectile and it is totally determined by the emission energy ($W$).

For heavier projectiles, which have greater charges, the perturbation $Z_p/v_p$ is stronger than that due to protons, so another approximation with a weaker perturbation should be used for determining ionization cross sections at relatively low ion speeds, say a few hundred keV/u. This is the case of the Continuous Distorted Wave-Eikonal Initial State (CDW-EIS) approximation [4, 5]. This approximation accounts for the influence of both the target and projectile on the emitted electrons so that, besides the binary peak, another structure is observed in electron angular distributions, the electron-capture into the continuum peak. This allows to reproduce the increase in the double differential cross section when the electron is emitted near 0-degree polar angle and at the same projectile speed. The CDW-EIS approximation is capable of rendering the so-call two center effects. Both the binary and ECC peaks will be discussed in detail below, when showing experimental ionization differential cross sections.

## 2. Experimental ionization cross sections

To the best of our knowledge, the first experiment involving energetic ions impacting on water has been performed by Toburen and colleagues in 1968 [6]. They only reported total cross sections for electron capture and loss by protons and neutral hydrogen, respectively. We will come back to this work when dealing with charge-transfer cross sections. Almost ten years later, Toburen and Wilson [7] performed a pioneer experimental work to determine water ionization cross sections due to the impact of fast ions. Specifically, they obtained absolute double and single differential cross sections for the ejection of electrons from water vapor bombarded by protons with energies of 0.3, 0.5, 1.0 and 1.5 MeV. Ejected electrons with energies ranging from a few eV to 5 keV were detected. Energy spectra of emitted electrons were obtained at polar angles covering the interval 15°-125°. The experimental setup they used is described in detail in a previous work [8]. Incident protons were accelerated by a Van de Graaff generator. The uncertainty of the absolute cross sections was estimated as ± 20 % for ejected electron energies above 10 eV. These authors concluded that data for electron energies less than 10 eV are not reliable due to technical problems with the electrostatic analyzer at such low energies. At the same time, they estimated that the uncertainty of absolute cross sections for 5 eV electrons was 200 %. Double differential ionization cross sections as a function of the emission angle are shown in Fig. 2 for proton energies of 0.3, 0.5, 1.0, and 1.5 MeV and for a few ejected electron energies. Structures such as the binary encounter (BE) peak can be observed, with a better delineation at high electron energies. Two-center or post-collisional effects can be also noticed in this figure. The influence of the electron capture to the continuum (ECC) peak is shown near the forward direction ($cos(\theta) \approx 1$) when the proton and electron velocities are close, as displayed in the curve corresponding to proton and electron energies of 0.5 MeV and 250 eV, respectively. At this proton energy, the electron energy is approximately 270

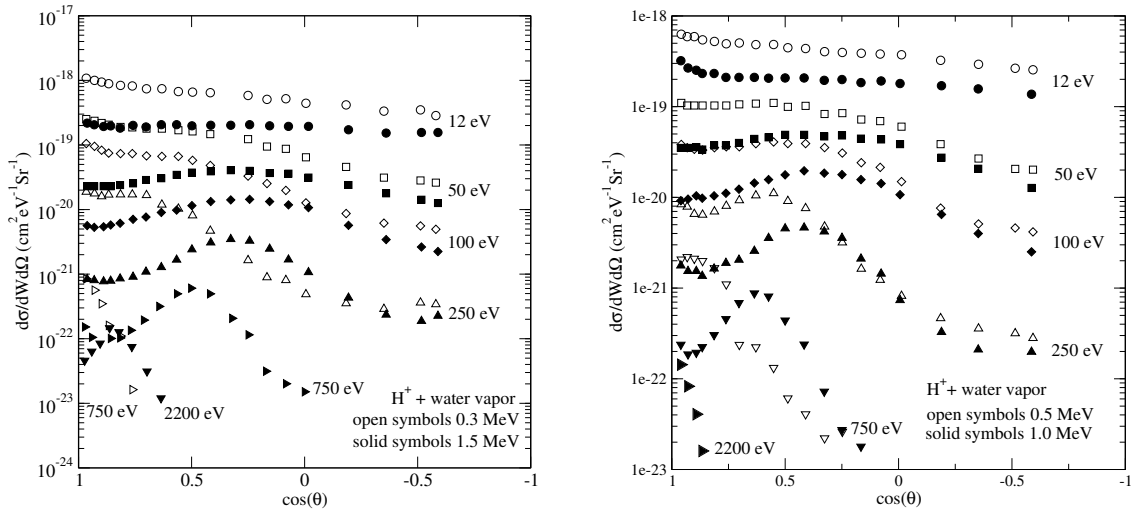


Figure 2: Double differential cross sections corresponding to electron emission after 0.3, 0.5, 1.0 and 1.5 MeV proton impact on water vapor. Data extracted from Ref. [7].

eV when both particles move with the same speed. An increase in the cross section is observed near 0° for the 250 eV curve. Another post-collisional effect is the asymmetry present in these angular distributions, with an evident cross section increase towards the forward electron direction. This behavior is caused by the electrostatic attraction existing between the electron and the proton after the collision. Additionally, as the proton energy increases, the low-energy electron angular distributions are more isotropic. Moreover, the BE peak is mor pronounced and narrower at high electron energies. On the one hand, the higher the proton energy, the weaker the post-collisional effects experienced by the emitted electron. In this case, the electron emission is basically a one-center process and the angular distribution is almost isotropic, based on the fact that water molecules are randomly oriented in space. On the other hand, the greater the proton energy, the stronger the binary collision, which makes the binding effects on the electrons less important and the BE peak narrower. In this case, the quantum effects on the cross sections are relatively weak.

In addition, Toburen et al. [7] tested two additivity and scalability rules usually used to calculate the cross sections of a complex molecular target from the cross sections of the target constituents. We refer here only to the atomic-based additivity and scalability rule (see Fig. 10 of Ref. [7]). This rule is more successful at high proton energies and, for a fixed proton energy, the water vapor measurements are better described at high electron energies. A good agreement between directly measured and scaled cross sections is obtained near the well defined BE peak. As a conclusion, this rule is more effective when the molecular details of the target are less important.

Toburen and colleagues [9] used the same experimental setup (described in Ref. [8]) to determine double differential cross sections for the yield of secondary electrons after the impact of $He^+$ and $He^{2+}$ ions on water vapor. Studied incident energies were

0.2, 0.3, 0.4 and 0.5 MeV/u for both projectiles. In addition, a 0.075 MeV/u $He^+$ beam was used in the experiment. Electrons were detected at polar angles ranging from 10° to 125°. Single differential and total ionization cross sections were determined by integration of the measured DDCS and SDCS, respectively. The $Z_P^2$ scaling rule was also analyzed using previously reported data acquired for proton beams impinging on the same target [7]. The absolute uncertainty estimated for these cross sections was about ±20%. However, the relative uncertainty necessary to compare the $He^+$, $He^{2+}$ and $H^+$ beam results was thought to be ±10% because these determinations were obtained with the same experimental setup. Figure 4 displays electron angular distributions corresponding to few selected electron energies when water vapor is irradiated with 0.3 and 0.5 MeV/u $He^+$ and $He^{2+}$ beams. The $Z_P^2$-scaled data for protons having the same velocities as the alpha particles are also displayed in this figure. On the one hand, the low energy electron emission at all angles due to $He^+$ is considerably lower than that corresponding to the alpha particles, $He^{2+}$. This fact is attributed to the screening of the nuclear charge produced by the bound electron of the $He^+$ ion at large impact parameters. On the other hand, the behavior at intermediate electron energies is opposite when the electron bound to the $He^+$ ion is released with an energy close to zero in the projectile frame of reference. Note that these zero energy electrons have laboratory energies of approximately 163 and 272 eV corresponding to 0.3 and 0.5 MeV/u ion beams respectively. Also, the reader should be aware that the stripping of $He^+$ ions is more important at higher incident energies. In addition, the cross sections for both projectiles in the well-defined BE peak zone and at high electron emission energies, are very close. This suggests that the nuclear charge screening due to the bound electron is not important for low impact parameter collisions. The $Z_P^2$ scaling rule worked well, except where the ECC process is important, at forward angles and when the projectile and electron velocities are similar.

Wilson et al. [10] published single differential ionization cross sections for 3.0 and 4.2 MeV protons in water vapor using the experimental setup reported previously by Toburen et al. [8]. Such data in conjunction with previous results reported by Toburen and Wilson [7] for 0.5 and 1.5 MeV proton energies are shown in Fig. 5. It should be pointed out that data for electron energies below 10 eV are not reliable due to the technical reasons explained previously [7]. Furthermore, Wilson and co-workers reported additional technical problems to detect very low energy electrons produced with the highest proton beam energies of 3.0 and 4.2 MeV. Nevertheless, they stated that the cross sections reported above an electron energy of about 10 eV are reliable for all impact energies. Experimental peaks obtained around electron energies of approximately 500 eV are produced by Auger emission from the oxygen K-shell. For low proton energies, these peaks have low intensities because energy transfers large enough to ionize the oxygen K-shell are less probable for such low energies. Semiempirical formulae developed to calculate single differential cross sections were integrated to determine proton beam total ionization cross sections that are compared, in Fig. 8 of Ref. [10], with those obtained by Schutten et al. [11] for electron beams having the same velocity. This

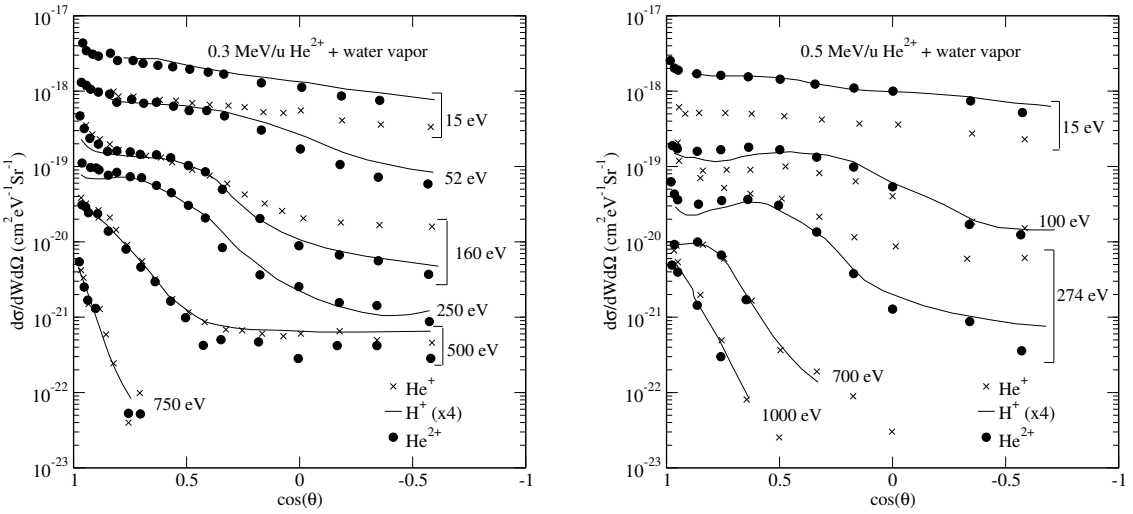


Figure 4: Angular distributions of selected electron energies emitted by water vapor due to the impact of (a) 0.3 and (b) 0.5 MeV/u $He^+$ and $He^{2+}$ ions. Corresponding data shown for protons [7] are $Z_P^2$-scaled. Reprinted from Publication [9], Copyright (1980), with permission from the Radiation Research Society.

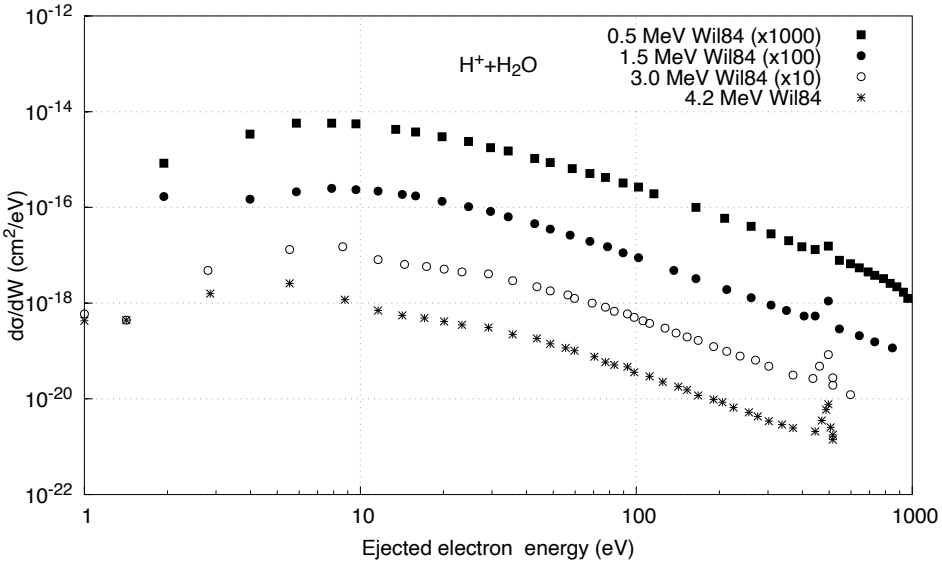


Figure 5: Single differential ionization cross sections for protons impacting on water vapor, with energies of 0.5, 1.5, 3.0, and 4.2 MeV reported by Wilson et al. [10].

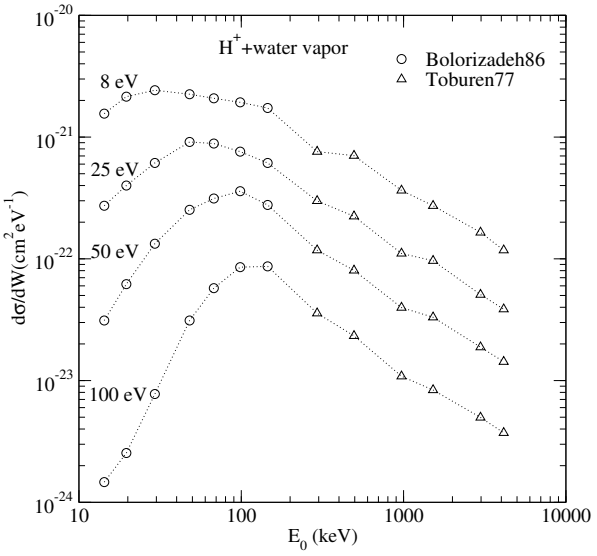


Figure 6: Single differential cross sections for electron emission after proton impact on water vapor as a function of the proton energy. Circles correspond to data published in reference [14] (Bolorizadeh86) and triangles to data obtained from Ref. [7] (Toburen77). Dotted lines are simply joining points.

comparison was made since proton beam data corresponding to water vapor were not available by the time of publication of Ref. [7] and, in addition, a previous work [12] had reported good agreement between the total ionization cross sections of incident protons and electrons of the same velocity at proton energies greater than about 0.5 MeV. At lower velocities, the positively charged projectiles have larger ionization cross sections than negatively charged particles having the same speed, probably due to target polarization effects [13].

In 1986, Bolorizadeh and Rudd published experimental absolute double differential cross sections for the ejection of electrons after the bombardment of water vapor with 15-150 keV protons [14]. Emitted electrons were detected at angles ranging from 10° to 160° and with energies varying from 1 to 300 eV. Their experimental configuration is fully described in an earlier publication [15]. Figure 6 displays single differential cross sections for the emission of electrons from proton-impacted water vapor as a function of the proton energy. These values were obtained after carrying out the angular integration of the double differential cross sections. These results complement those reported previously by Toburen et al. [7] since these works cover different proton energy regions. It is not clear how Bolorizadeh and Rudd determined cross sections from Toburen's work for incident energies above 1.5 MeV, the upper limit reported by the latter. It can be observed that Toburen's values at lower incident energies would tend to underestimate those reported by Bolorizadeh and Rudd. The region below a few hundreds of keV is very important to study: therein the First Born approximation loses its validity. The reader should notice that the single differential cross section maximizes at certain proton energy and that the position of the cross section maximum shifts toward lower proton energies as the electron energy decreases. This behavior can be attributed to the competition between electron capture by the projectile and the ionization phenomena. As the proton energy decreases, the electron capture process begins to be relevant and the electron ionization tends to decrease. In addition, this

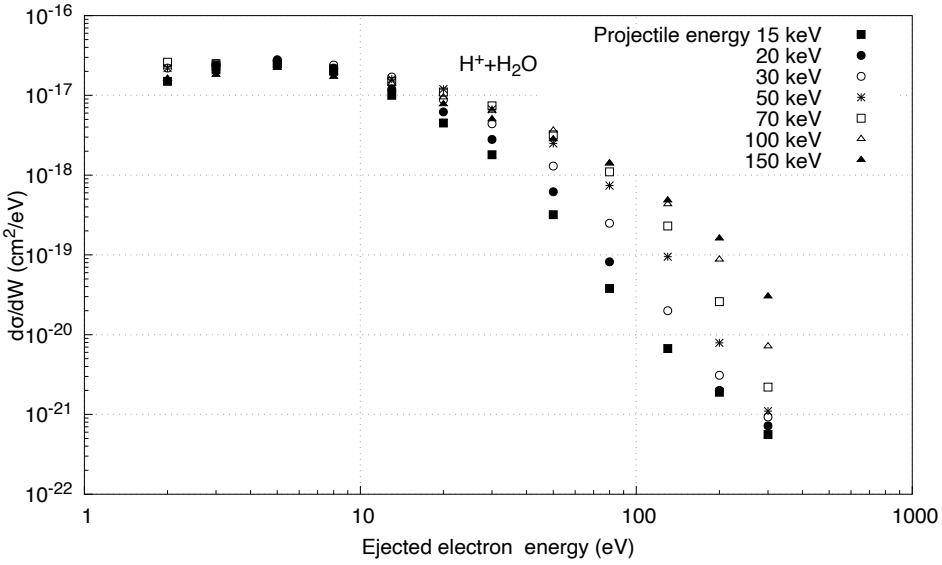


Figure 7: Single differential ionization cross sections for protons impacting on water vapor, with energies of 15, 20, 30, 50, 70, 100, and 150 keV, reported by Bolorizadeh and Rudd [14].

maximum in the SDCS as a function of the projectile energy is related to the so-called Massey peak. This peak appears when the projectile speed is similar to that of the atomic electron. In other words, when the projectile speed decreases too much, the collision time ($\sim b/v$, where b is the impact parameter and v the projectile speed) falls below the electron orbital characteristic period, and this weakens the inelastic coupling. This is the Massey adiabatic criterion. Then, below the Massey peak, energy transfer decreases and so do ionization cross sections. When the projectile speed is much higher than that of the orbital electron, the electron capture plays a negligible role. For clarity purposes, it is important to mention that electrons with energies of 8, 25, 50, and 100 eV are captured into the continuum, when proton energies are about 15, 46, 92, and 184 keV respectively.

Figure 7 shows single differential ionization cross sections reported by Bolorizadeh and Rudd, for proton energies ranging between 15 and 150 keV, well below the range studied by Wilson et al. [10]. Unlike Fig. 5, in which data series were scaled for better visualization, here the originally measured cross sections are shown. At higher electron ejection energies, ionization cross section increases with the projectile energy because a more energetic projectile can transfer more energy to bound electrons. It can be also observed that cross sections for the different proton energies converge to a similar value for very low electron ejection energies. At about 5 eV electron energy, differential cross section are within $(2.5\pm0.3) \times 10^{-17} cm^2$. According to these results, differential cross sections for the emission of very low energy electrons, that are produced by dipole (weak) transitions, are almost independent of the projectile speed. In other words, the First-Born (B1) approximation does not hold at such low projectile energies. These very

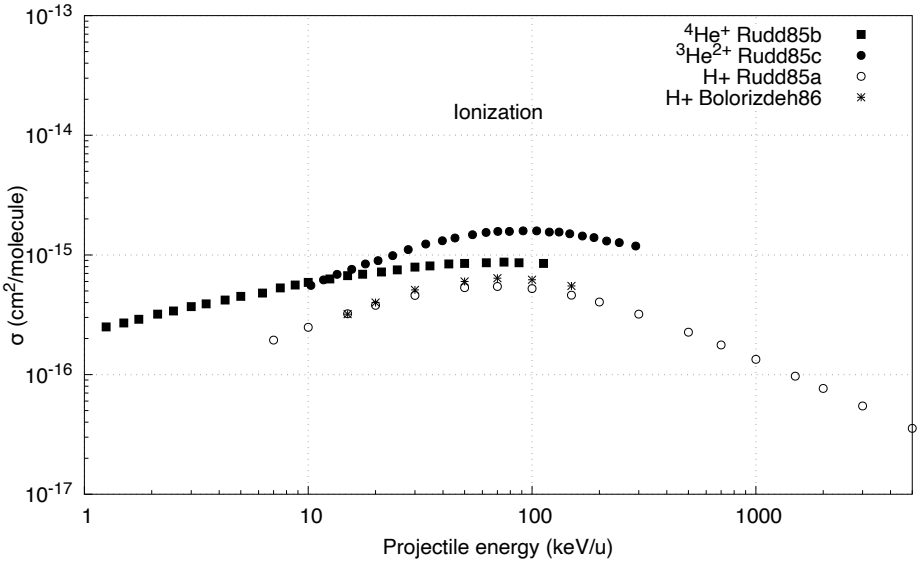


Figure 8: Total ionization cross sections for protons, $He^+$, and $He^{2+}$ particles, as a function of the specific energy (speed), as reported by Rudd et al. [16, 17, 18] and Bolorizadeh and Rudd [14].

low energy electrons are produced by collisions with large impact parameters and are emitted with nearly isotropic angular distribution, as shown in Fig. 2.

Total ionization cross sections obtained by Bolorizadeh and Rudd are shown in Fig. 8, in conjunction with those reported previously by Rudd et al. [16, 17, 18]. For protons, results show a very good agreement. Proton and $He^+$ cross sections would be similar at the same projectile speed if the First-Born approximation holds. In this case, such cross sections are close to one another near the Massey peak and may converge to similar values at high projectile speed but data for the $He^+$ ions go up to 100 keV/u only, an energy not high enough to observe the B1-convergence. As expected, the largest cross sections are obtained for alpha particles when compared with those for protons and $He^+$ ions, since alpha particles have a higher charge. For instance alpha particles and protons at 300 keV/u have cross sections of $11.9 \times 10^{-16} cm^2$ and $3.2 \times 10^{-16} cm^2$, respectively. This means that $\sigma_\alpha/\sigma_p \sim 3.7$, which is similar to the expected factor of 4 due to charge scaling (see the comments on eq. (10)). Taking into account the uncertainties of about 19 % for the values reported by Bolorizadeh and Rudd, it can be said that the B1 approximation holds at such projectile speed.

A Japanese research group led by D. Ohsawa carried out experiments to study ionization cross sections corresponding to $He^{2+}$ and carbon ions bombarding water vapor. Their experimental setup was detailed in Ref. [19]. An extended analysis of their results was done in a separate paper [20] for 6.0 and 10 MeV/u $He^{2+}$. It is important to mention that the data for 6 MeV/u carbon ions have been referenced in a theoretical work published later [21]. The DDCS values were reported for ejected electron energies in the intervals 7-10 000 eV and 20-14 000 eV for 6.0 and 10.0 MeV/u $He^{2+}$ ion beams

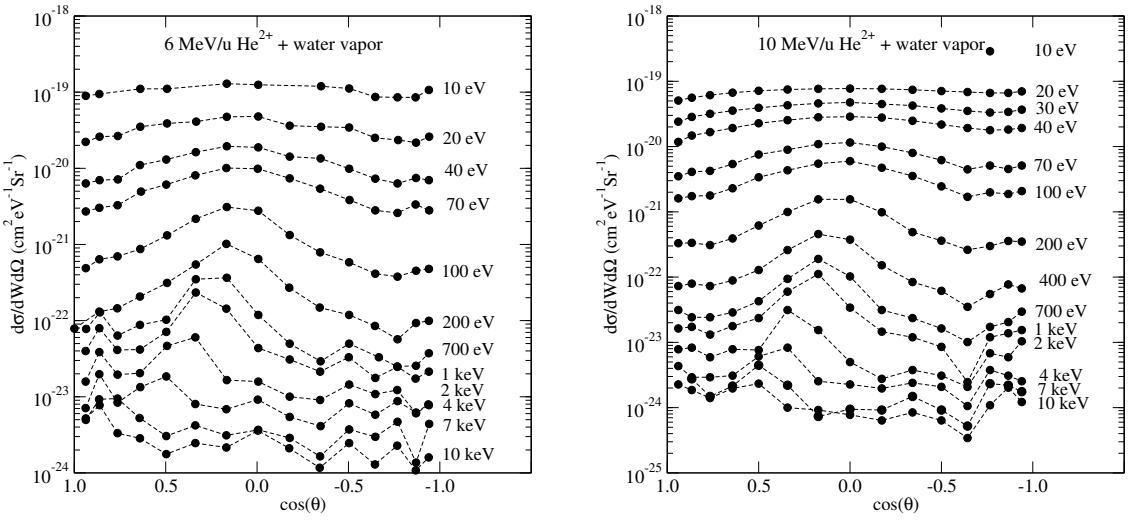


Figure 10: Double differential cross sections for electron emission from water vapor bombarded by a) 6 MeV/u and b) 10 MeV/u $He^{2+}$ ions. Values extracted from Ref. [20].

respectively, and at emission angles ranging from 20° to 160° (see Fig. 10). Besides, the SDCS results were calculated by extrapolating the angular distributions to polar angles beyond the interval mentioned above. A systematic uncertainty was estimated to be ±13 % for all angles and energies. However, for 6.0 MeV/u projectiles, the statistical uncertainty was about 1% at electron energies lower than 100 eV and climbed up to several ten percent at about 10 keV. These uncertainties were about 30% in the 40°-140° interval and as high as 80% at 20° and 160°. These authors calculated relativistic electron energies corresponding to the BE peak for a few angular positions and compared them with those obtained from their experiment and the investigation carried out by Toburen et al. [9] at 0.4 and 0.5 MeV/u energies. Both experiments produced the BE-peak energies lower than the theoretical ones. Absolute shifts corresponding to the work of Toburen did not change very appreciably either with the angular position or the projectile energy (see Table 1 of Ref [20]). On the contrary, the shifts reported by the Japanese group decrease as the emission angle increases and are lower at the highest projectile energy (10 MeV/u). We want to point out that the relative shift, defined as the ratio between the absolute energy shift and the experimental BE-peak energy, is the same within the uncertainty for all emission angles at a given projectile energy. Ohsawa et al. [20] speculated that this behavior could be caused by electron binding effects, the ECC phenomenon and the finite angular resolution of the detection system, without quantifying the contribution of each of these causes. It is good to mention that the ECC process has little influence on DDCS at angles more than about 30° for this combination of projectile charge and velocity.

Another important issue related to this work is the unexpectedly high electron emission at backward angles greater than 130°. They explained this as a consequence of the so-called Fermi shuttle acceleration [22]. Nothing is said about either the oscillation

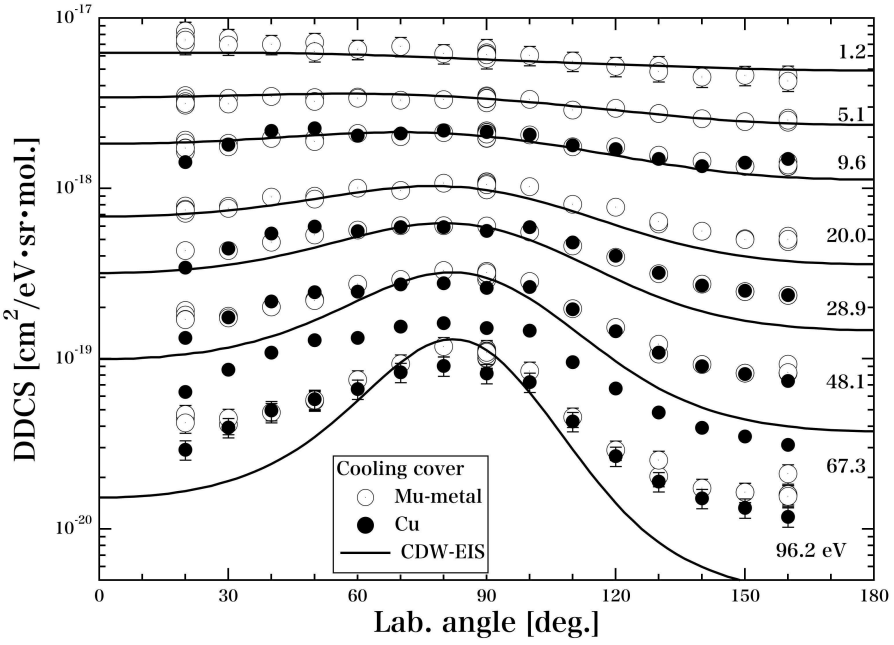


Figure 11: Double differential cross sections for electron emission from water vapor bombarded by 6 MeV/u $C^{6+}$ ions [23]. Reprinted with permission of the Institute of Physics.

observed in the angular distribution at angles greater than 90° for 6.0 MeV/ u projectiles or the absolute minimum present at 130° for the 10.0 MeV/u ion beam and almost all electron energies (see Fig. 10). In our opinion, the large uncertainties quoted in the article considered here at high emitted electron energies make the analysis of results difficult.

After improving the experimental setup, the Ohsawa's group has recently presented a work in which double differential cross sections for water vapor ionization by 6 MeV/u $C^{6+}$ ions were reported [23]. Now, DDCS for the emission of electrons with energies down to ∼1 eV can be determined. Figure 11 shows these cross sections for electrons emitted with energies within the interval 1-100 eV. Corresponding theoretical predictions according to the Continuum Distorted Wave-Eikonal Initial State approximation are also depicted. It is evident that this theoretical approach underestimates forward and backward cross sections as the emitted electron energy increases.

## 3. Experimental charge-transfer cross sections

Toburen et al. measured charge-transfer cross sections for protons and hydrogen atoms interacting with several gaseous targets [6]. For water specifically, cross sections were determined for impact energies from 10 keV up to 2500 keV. The combined uncertainties reported for electron capture and loss cross sections are about 10 % and 12 %, respectively. Charge-states of outgoing projectiles were analyzed as a function of the gas cell pressure so that charge-transfer cross sections could be determined. Solid-state

detectors were used to accomplish this task.

Rudd and colleagues carried out an experiment to determine total cross sections for the production of negatively ($\sigma_-$) and positively ($\sigma_+$) charged particles after the impact of 7-4000 keV protons on water vapor [16]. As far as we understand, these authors supposed that no negatively charged product was generated, except electrons. On the one hand, this means that the production of a negative particle would be only possible after the release of an electron to the continuum from the target molecule. Therefore, they stated that $\sigma_-$ is equivalent to the total ionization cross section. On the other hand, positive ions would be only created after the emission or transfer of an equal number of electrons. In addition, these authors mentioned explicitly that the double capture phenomenon was not accounted for. For these reasons, they proposed to calculate the electron capture cross section using the formula $\sigma_{10} = \sigma_+ - \sigma_-$, which is a plausible method under such conditions. Beams produced from four accelerators were used in this study with parallel-plate capacitor detectors setup to collect particles with different charges states. The details of the experimental configuration and procedures can be found in a previous publication [24]. Estimated uncertainties corresponding to $\sigma_{-,+}$ ranged from about 20 % at 10 keV to 8% above 500 keV while the $\sigma_{10}$ uncertainty was observed to be higher, especially when the difference between $\sigma_+$ and $\sigma_-$ was small, reaching a value of 60% at 100 keV. For this reason, electron capture cross sections were not reported in Ref. [16]. However, we have applied this formula for estimating $\sigma_{10}$ and the corresponding results will be shown and discussed just below.

A similar work was published by a group led by Rudd [17] reporting experimental cross sections for ionization and electron capture and loss for 5-450 keV $^4He^+$ beams impinging on water vapor. They followed the same methodology used before [16], where cross sections for electron and positive ion production were obtained from data gathered from two accelerators only. In addition, they used an electrostatic selector to steer neutral, singly and double charged components towards three independent detectors. In this case, they used the expression $\sigma_+ - \sigma_- = \sigma_{10} - \sigma_{12}$ to fit the data, where $\sigma_{10}$ and $\sigma_{12}$ are electron capture and loss cross sections respectively. This formula assumes that the double electron capture cross section is negligible. Figures 13 shows the experimental results reported in Refs. [16, 17] and Table 1 of the mentioned publication contains the corresponding values. Reported uncertainty intervals were 8-12% for $\sigma_+$, 5-12% for $\sigma_-$, 13-53% for $\sigma_{12}$, and 11-12% for $\sigma_{10}$.

Figure 12 shows electron capture $\sigma_{10}$ and loss $\sigma_{01}$ cross sections obtained by Toburen et al. [6] for protons and hydrogen atoms, respectively, when impacting on water vapor. In addition, $\sigma_{10}$ obtained from the data reported by Rudd et al., for $\sigma_+$ and $\sigma_-$ [16], was also included. It should be remarked that the Rudd's $\sigma_{10}$ values seem to complete those published by Toburen et al. for energies below 100 keV. Above this energy, Rudd's values overestimated those from Toburen et al. and should not be considered due to their very high uncertainty, as explained by Rudd et al. [16]. Values for $\sigma_{10}$ obtained by Rudd et al. [17] for $^4He^+$ are also shown at the same projectile speed as protons. It can be observed that $\sigma_{10}$ for protons and $^4He^+$ are similar at the same speed, as it would

expected from the First Born approximation, where cross sections depend only on the projectile charge and speed. However, this approximation should not be valid for specific energies below 100 keV/u for a unity-charge projectile and other effects related to the electron bound to the projectile may arise. It can be observed that electron capture cross section increases as the projectile energy decreases, then a maximum is achieved. As explained in the introduction section, this maximum is due to the matching of the projectile and orbital electron speeds. Here it is also observed that electron loss cross section decreases with the projectile energy but it has to be remarked that this occurs for energies above about 100 keV/u. For lower energies, this cross section increases with the projectile energy. That is, there is a maximum around 80-100 keV/u, which depends on the molecule target in question, as it can be seen in the Toburen's work [6]. Below, this issue will be treated again for the electron loss from $^3He^+$ ions (see Fig. 13. and the accompanying discussion).

There is another important work on charge transfer cross sections published by Rudd et al. for $^3He^{2+}$ impacting on several gaseous targets, including water, in the 5-150 keV/u specific energy range [18]. They used the same experimental setup as in Refs. [16, 17] and they measured one- and two-electron capture cross sections $\sigma_{21}$ and $\sigma_{20}$, respectively, in addition to $\sigma_+$ and $\sigma_-$. Assuming that three-electron capture is negligible, charge conservation leads to $\sigma_+ = \sigma_- + \sigma_{21} + \sigma_{20}$. The authors used the isotope $^3He$ for avoiding confusion with $H_2^+$, which has the same charge to mass ratio as $^4He^{2+}$ and is very difficult to remove from the collision chamber. Figure 13 displays the complete set of charge transfer cross sections for the different He charge states, except for $He^0$ ($\sigma_{01}$ and $\sigma_{02}$). Electron cross sections for $H^0$ were also included in this plot to show the high-energy behavior that would be observed for $^3He^+$, and vice-versa. Of course, the loss of an electron from $^3He^+$ would be less likely than from a $H^0$ atom since the electron binding energy in the former is four times that in the latter. This factor of 4 comes from the $Z^2$ scaling of the binding energy in a hydrogen-like atom, where $Z$ is the nucleus charge.

When an ion beam interacts with matter, a dynamical equilibrium between the possible charge states is established at each projectile energy. Knowing charge transfer cross sections allows the determination of charge fractions and so the beam charge expected value. Charge balance equations can be written for a given ion. For protons, they are

$$-\sigma_{01}\Phi_0 + \sigma_{10}\Phi_1 = 0 \tag{11}$$

$$\Phi_0 + \Phi_1 = 1, \tag{12}$$

where $\Phi_0$ and $\Phi_1$ are the charge-state fractions corresponding to $H^0$ and $H^+$, respectively. For alpha particle, where 3 charge states are possible, we get

$$-(\sigma_{01} + \sigma_{02})\Phi_0 + \sigma_{10}\Phi_1 + \sigma_{20}\Phi_2 = 0$$

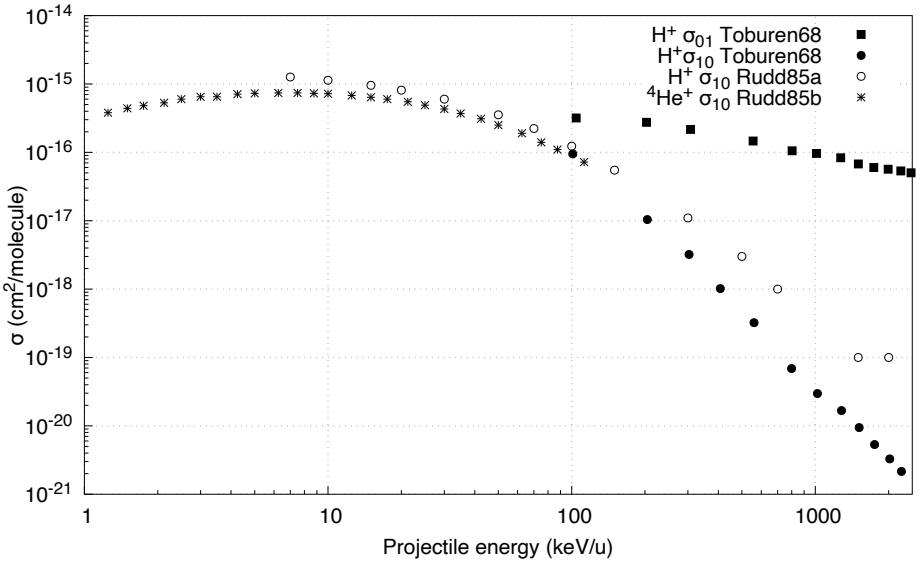


Figure 12: Electron capture and electron loss cross sections for proton impacting on water vapor as experimentally determined by Toburen et al. [6] and Rudd et al [16]. Electron capture cross section for $^4He^+$ was also included for comparison with those determined for protons at the same speed.

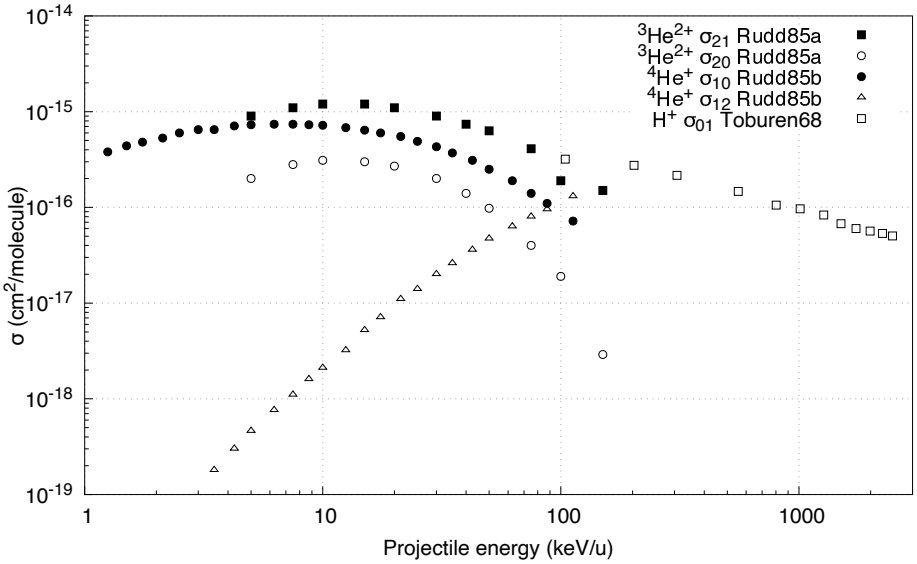


Figure 13: Electron capture and electron loss cross sections for $^3He^{2+}$ and $^4He^+$ particles impacting on water vapor as experimentally determined by Rudd et al [17, 18]. Electron loss cross section for $H^0$ determined by Rudd et al. [16] is also included for showing the high energy behavior for this process.

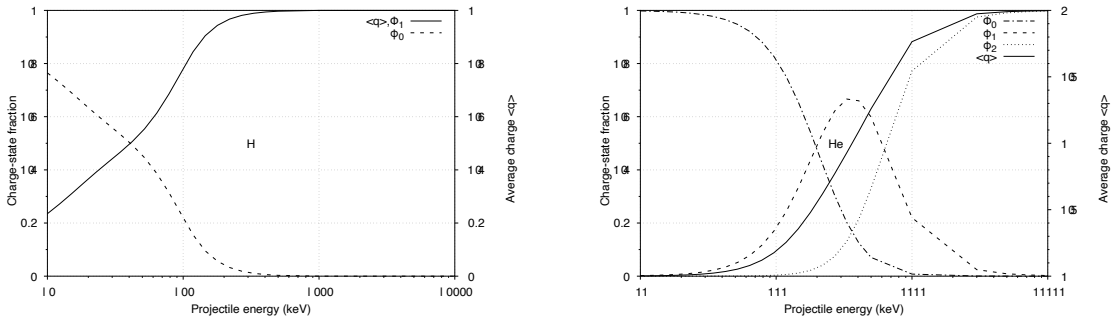


Figure 15: Charge-state fractions and charge expected values as a function of the projectile energy for Hydrogen (a) and Helium (b) atoms interacting with water [25].

$$\begin{aligned} \sigma_{01}\Phi_0 - (\sigma_{10} + \sigma_{12})\Phi_1 + \sigma_{21}\Phi_2 &= 0 \\ \Phi_0 + \Phi_1 + \Phi_2 &= 1. \end{aligned}$$

Bernal [25] used these equations and charge-transfer cross sections, and determined charge-state fractions and charge expected values for Hydrogen and Helium atoms. Figure 15 shows the results of such calculations. In general, slower projectiles have lower expected charge, and vice-versa since fast atoms are stripped during collisions with target molecules.

For more details on the electron capture process, the reader is advised to read the work recently published by Belkić [26]. He determined cross sections for this process when protons impact several targets with biological interest, like water and DNA bases. This was done by applying the Continued-Distorted Wave approximation to several atoms and using the Bragg additivity rule for calculating cross sections for the molecule in question. This rule uses atomic cross sections and combines them for obtaining molecular cross sections, weighting each atomic results by the number of the corresponding atom in the molecule. This procedure neglects molecular binding but it has been shown to provide consistent results. A few experimental values of electron capture cross section for DNA bases are also reported. The reader may be also interested in reading the comprehensive review on the ionization problem published also by Belkić in 2010 [27]. There, distorted wave approximations for determining ionization cross sections are reviewed. That approach can be used in conjunction with Slater-type wave functions for atoms into molecular targets, which can be seen as a step further the Bragg additivity rule. However, this rule may be useful for determining molecular cross sections from atomic cross sections, used in Monte Carlo codes. Also, he comments on the extension of distorted wave approximations to the relativistic regime, which can be necessary when dealing with proton beams used for treating deep-seated tumors.

Although ionization and charge-transfer cross sections for other media different from water are out of the scope of this review, it is good to draw the reader's attention to a recent review published by Tribedi [28] on ionization and fragmentation of large biomolecules by the impact of heavy charged particles, including protons and carbon

ions, among other heavy ions. Commonly, these experiments use a Time-of-Flight spectrometer to resolve target fragments produced by ion impact, in conjunction with an electron analyzer. As Wilson et al., Tribedi argues that the decrease of ionization SDCS for secondary electrons with energies below ∼10 eV, seems to be non physical.

This review is an opportunity to discuss this issue that, up to our knowledge, was firstly raised by Wilson et al. [10] (see Fig. 5 and related comments). Inelastic collision can be decomposed into two stages, first the projectile transfers some momentum to the electronic target, atom or molecule, and then the target distributes this momentum among the possible electronic transitions, namely excitations or ionizations. The probability for each transition is given by the Generalized Oscillator Strength (GOS) [29]. Low energy electrons are produced by optical transitions, that is for low momentum transfers which correspond to large impact parameter collisions. In this situation, the GOS reduces to the Optical Oscillator Strength (OOS). Such distant collisions contribute with higher differential cross sections for momentum transfer so it could be expected that SDCS for ionization would increase as the secondary electron decreases. However, after integrating the OOS over the momentum space, it can be observed that it increases as the energy transfer decreases up to a region where it decreases again, conforming a maximum. This means that below a certain value, the probability for energy transfers decreases again so that SDCS as a function of the secondary electron energy may decrease below ∼10 eV for water. We have calculated the optical absorption spectrum for a DNA base-pair using the Time-Dependent Density-Functional Theory [30, 31] and it is shown in Fig. 16. Discrete or excitation transitions have been smoothed out during the averaging of this cross section for optical excitations along the three main cartesian axes. This is a molecule much more complex than water but it can be used to explain our point. Water would show the same behavior. It can be observed that this cross section shows a maximum around 17 eV, region that is related to the so-called collective oscillations in which all the electrons oscillate as in a plasma. This energy is also known as the plasmon energy, that is about 21 eV for liquid water [32]. Thus, it could be expected that SDCS would decrease for energy transfers below ∼21 eV in water. Taking into account that the outermost and leading water orbital has a binding energy of about 11 eV, then the ionization SDCS as a function of the secondary electron energy would decrease below ∼10 eV. This is what has been observed in the experimental results reported by Wilson et al. [10] and Tribedi [28]. According to our theoretical analysis, this experimental observation may have physical plausibility.

## 4. Water fragmentation analysis

A very sophisticated experiment was carried out by Werner et al. [33] where multiple ionization and fragmentation of the water molecule after the bombardment with 100-350 keV protons and 250 keV $He^{2+}$ particles were studied. They were able to detect up to five fragments in coincidence and determined cross sections for the production of the $H_2O^+$, $H^+$, $OH^+$, and $O^+$ ions. Since this experiment was only sensitive to positive

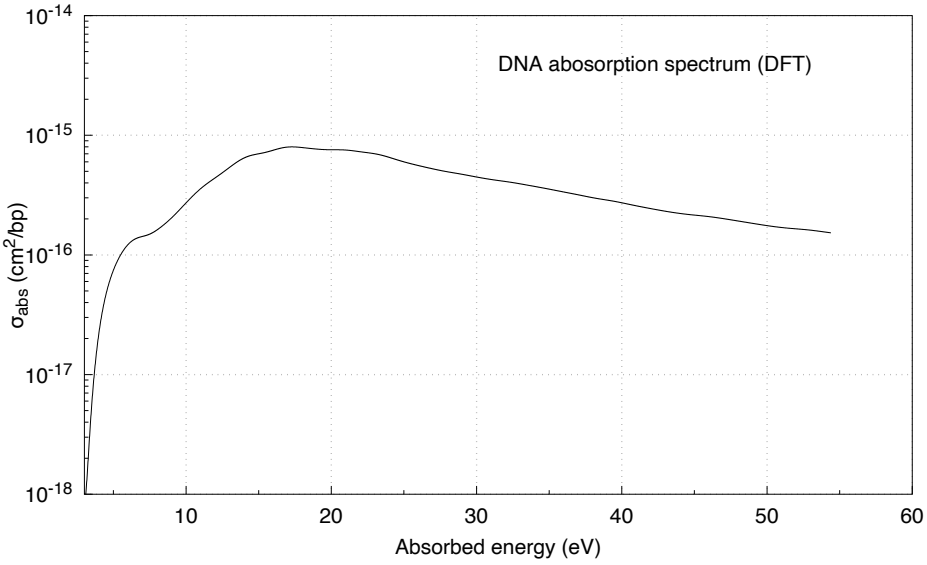


Figure 16: Optical absorption cross section for a DNA base-pair calculated using the Time-Dependent Density-Functional Theory (not published).

ions, reactions where $O^+$ and $O^0$ were produced could not be resolved. For this reason, the previous assumption made by Rudd et al. [16] that no negative radical is generated during water fragmentation by proton impact, could not be confirmed. Emphasis was put on the study of the complete fragmentation processes $H_2O \rightarrow H^+ + H^+ + O^+ + 3e^-$ and $H_2O \rightarrow H^+ + H^+ + O^{2+} + 4e^-$. Total cross sections obtained in this work for positive ion production were compared to those reported by Rudd et al. [16].

Gobet and co-workerc [34] (see also Ref.[35]) have recently carried out a detailed experiment to study the water ionization by protons with energies ranging from 20 to 150 keV. They detected water-product charge states in coincidence with those of the projectile and they discriminated between the following ionization mechanisms: direct ionization, single electron capture and double electron capture. A time-of-flight (TOF) mass-to-charge spectrometer was used to determine which product ions were produced in coincidence with the corresponding hydrogen charge state detected after passing through another mass-to-charge spectrometer. The latter spectrometer allowed to eliminate ions such as $H_2^+$, $H_3^+$ and others originated from impurities in the source. In this work, $H_2O^+, OH^+, O^+, O^{2+}$, and $H^+$ ions were the detected. The authors reported for the first time the detection of $H_2^+$ fragments after protons impacting on water and confirmed the previous finding by Rudd et al. [16] that anions are not observed after this kind of collisions. Figure 17 displays total and partial absolute ionization cross sections for water molecule fragmentation after proton impact, as determined by those authors. Partial cross sections are discriminated according to the water fragment produced. Solid and open symbols represent experimental values reported by them and those determined by Werner et al. [33] respectively. Lines correspond to fits obtained by using a formula reported by Rudd et al. for $\sigma_-$ [16] and the corresponding parameters can be found in

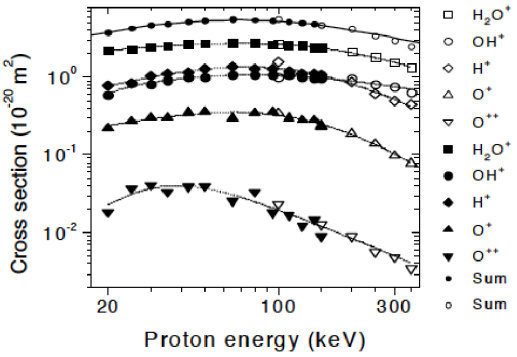


Figure 17: Total and partial absolute cross sections for water molecule fragmentation after proton impact. Solid and open symbols represent experimental values reported by Gobet et al. [34] and Werner et al. [33] respectively. The lines correspond to fits generated by using the formula reported by Rudd et al. for $\sigma_-$ [16]. Reprinted figure with permission from Publication [34]. Copyright (2004) by the American Physical Society.

the article under analysis [34] . The total ionization cross section and its discrimination between ionization and electron capture processes are shown in Figure 18. Circles and squares represent experimental values reported by Gobet et al. [34] and triangles are data published by Werner et al. [33]. The curves are fits for the total and ionization CS determined from the expressions developed by Rudd et al. for $\sigma_+$ and $\sigma_-$ respectively [16]. According to this work, ionizations and single electron captures contribute roughly the same to the total ion production at 50 keV proton energy. Below this energy, the total ion yield is dominated by electron captures and above, by ionizations (see Fig. 5 of Ref. [34]).

It is important to remark that Gobet *el al.* reported a local minimum and an absolute maximum in the ionization and electron capture cross sections, respectively (see Fig. 2 of Ref. [35]). They argued that the competition between these processes is responsible for this behavior. However, this reason may not be enough to explain these observations. It is interesting that the minimum and maximum mentioned above were not reported in their last publication (see Fig. 18). In addition, uncertainties were not reported in both articles, which makes an analysis of their results more difficult. Despite these facts, data reported in the publications under consideration can be very useful for researchers that use numerical simulations to study indirect DNA damage caused by ionizing radiation.

Luna et al. [36] studied the water molecule fragmentation after the impact of $H^+$ ions with energies of 15 to 100 keV and 500 to 3500 keV, and of 8 to 100 keV $H^0$ projectiles. Absolutes cross section for various water fragmentation channels after ionization and electron capture processes were determined using coincidence analysis. A detailed analysis on the decaying channels after the impact of the involved projectiles is provided by these authors. They concluded that ionizations occur mainly in outer shells at high impact energies. At lower projectile energies, valence electron captures and ionizations dominate over transfer ionizations. They also showed that $H^+$ ions are as efficient as $H^0$ projectiles to ionize the water molecule. This fact is very important when studying the relative biological effectiveness of proton beams near the Bragg peak.

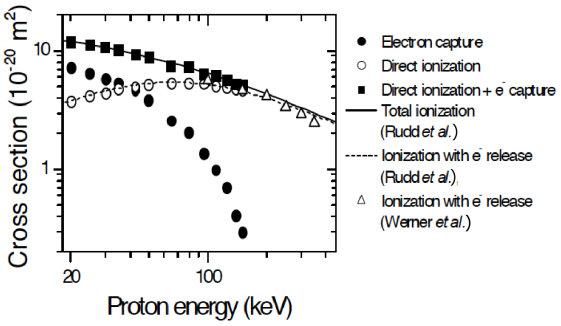


Figure 18: Total ionization cross sections discriminating between electron capture and direct ionization for proton impact on water vapor. Circles and squares represent the experimental values reported by Gobet et al. [34] and triangles are analogue data published by Werner et al. [33]. The lines represent fits obtained from the expressions published by Rudd et al. [16]. Reprinted figure with permission from Publication [34]. Copyright (2004) by the American Physical Society.

## 5. Conclusions

Cross sections for water ionization by ion impact are rather scarce in spite of having into account the enormous importance of this medium for life. In addition, available CS have been determined in water vapor due to the experimental difficulties associated to the arrangement of a liquid target and the collection of the electrons produced within such a medium, mainly the low energy electrons that may not even escape from the target. A few experimental works have studied the electron emission from amorphous solid water (ASW) after the impact of swift ions [37, 38]. Similar efforts have been made for electron impact on ASW [39]. Although these experimental works are unable to provide absolute ionization cross sections, they reported very important data for benchmarking Monte Carlo (MC) codes for couple ion-electron transport simulations in condensed water. Unfortunately, discrepancies between the electron emission yields determined by experiments and MC simulations are still large.

Charge-transfer is another important physical process when ions impact matter since they can capture or lose electrons. During these processes, ion charge changes and so the corresponding interaction cross sections. As reviewed here, experiments for determining these cross sections for energetic ions in water are also scarce and have been determined mainly for protons and $He^{2+}$ in the gas phase only. More efforts should be made for updating experiments with these projectiles and include other light and heavy ions, like carbon ions.

Experiments on water fragmentation after ion impact are also very important as they provide useful information about the products of the ion-water collision process and the possible channels by which intermediate water species can decay. This information is important for studies on the biological relative effectiveness of ion beams as the main component of the DNA strand break comes from the attack of chemical species produced by water radiolysis.

Additional efforts should be made to obtain experimental cross sections for liquid water ionization. Such data are of primordial importance for research on biomedical applications of ion beams. On the one hand, human being is mainly composed by liquid water. On the other hand, ionizations are responsible for secondary electron

emission and, indirectly, for reactive chemical species production by water radiolysis, both responsible for most of the DNA damage after ionizing radiation impact.

## 6. Acknowledgments

M. A. Bernal thanks the FAPESP foundation in Brazil for financing his research activities through the projects 2011/51594-2, 2015/21873-8, 2018/15316-7, and 2020/08647-7. In addition, he acknowledges the financial support received from the CNPq through the 306298/2018-0 fellowship.

## 7. References

[1] M. McDowell, J. Coleman, Introduction to the Theory of Ion-Atoms Collisions, Amsterdam: North-Holland, 1970.

[2] ICRU49, Stopping powers and ranges for protons and alpha particles, Tech. rep., International Commission on Radiation Units and Measurements, Bethesda, MD (1993).

[3] J. P. Hansen, L. Kocbach, Ejection angles of fast delta electrons from k-shell ionisation induced by energetic ions., J. Phys. B 22 (1989) L71–L77.

[4] D. Crothers, J. McCann, Ionisations of atoms by ion impact, J. Phys. B 16 (1983) 3229–3242.

[5] D. Belkic, Leading distorted wave theories and computational methods for fast ion–atom collisions, Journal of Computational Methods in Sciences and Engineering 1 (1) (2001) 1–73.

[6] L. H. Toburen, M. Y. Nakai, R. A. Langley, Measurement of high-energy charge-transfer cross sections for incident protons and atomic hydrogen in various gases, Physical Review 171 (1) (1968) 114–122.

[7] L. H. Toburen, W. E. Wilson, Energy and angular distributions of electrons ejected from water vapour by 0.3-1.5 MeV protons., J Chem Phys 66 (1977) 5202–13.

[8] L. H. Toburen, Distributions in energy and angle of electrons ejected from molecular nitrogen by 0.3- to 1.7-MeV protons, Physical Review A 3 (1) (1971) 216-228.

[9] L. H. Toburen, W. E. Wilson, R. J. Popovich, Secondary electron emission from ionization of water vapor by 0.3 to 2.0 MeV $He^+$ and $He^{2+}$ ions., Rad. Res. 82 (1980) 27–44.

[10] W. E. Wilson, J. H. Miller, L. H. Toburen, S. T. Manson, Differential cross sections for ionization of methane, ammonia and water vapour by high velocity ions., J Chem Phys 80 (1984) 5601–5608.

[11] J. Schutten, F. J. DeHeer, H. R. Moustafa, A. J. H. Boerboom, J. Kistemaker, Cross and partial ionization cross sections for electrons on water vapor in the energy range 0.1-20 keV., J. Chem. Phys. 44 (1966) 3924–3928.

[12] J. W. Hooper, D. S. Harmer, D. W. Martin, E. W. McDaniel, Comparison of electron and proton ionization data with the born approximation predictions., Phys. Rev. 125 (6) (1962) 2000–2004.

[13] K. P. et al, Ionization of rare gases by particle - antiparticle impact, Journal of Physics B: Atomic, Molecular and Optical Physics 30 (17) (1997) L581.

[14] M. A. Bolorizadeh, M. E. Rudd, Angular and energy dependence of cross sections for ejection of electrons from water vapor. ii. 15-150-keV proton impact, Physical Review A 33 (2) (1986) 888–892.

[15] M. E. Rudd, T. Jorgensen, Energy and angular distribution of electrons ejected from hydrogen and helium gas by protons, Physical Review 131 (2) (1963) 666-675.

[16] M. E. Rudd, T. V. Goffe, R. D. Dubois, L. H. Toburen, Cross sections for ionization of water vapor by 7-4000 keV protons., Phys. Rev. A 31 (1) (1985) 492–494.

[17] M. E. Rudd, A. Itoh, T. V. Goffe, Cross sections for ionization, capture, and loss for 5-450 keV $He^+$ on water vapor, Phys. Rev. A 32 (4) (1985) 2499–2500.

[18] M. E. Rudd, T. V. Goffe, A. Itoh, Ionization cross sections for 10-300-keV/u and electron-capture cross sections for 5-150-keV/u $^3He^{2+}$ ions in gases, Physical Review A 32 (4) (1985) 2128–2133.

[19] D. Ohsawa, H. Kawauchi, M. Hirabayashi, Y. Okada, T. Honma, A. Higashi, S. Amano, Y. Hashimoto, F. Soga, Y. Sato, An apparatus for measuring the energy and angular distribution of secondary electrons emitted from water vapor by fast heavy-ion impact, Nuclear Instruments and Methods in Physics Research Section B: Beam Interactions with Materials and Atoms 227 (3) (2005) 431–449.

[20] D. Ohsawa, Y. Sato, Y. Okada, V. P. Shevelko, F. Soga, 6.0-10.0 MeV/u $He^{2+}$ -ion-induced electron emission from water vapor, Phys. Rev. A 72 (2005) 062710.

[21] C. Dal Cappello, C. Champion, O. Boudrioua, H. Lekadir, Y. Sato, D. Ohsawa, Theoretical and experimental investigations of electron emission in C6+-H2O collisions, Nuclear Instruments and Methods in Physics Research Section B: Beam Interactions with Materials and Atoms 267 (5) (2009) 781–790.

[22] E. Fermi, On the origin of the cosmic radiation, Physical Review 75 (8) (1949) 1169–1174.

[23] D. Ohsawa, H. Tawara, T. Okada, F. Soga, M. E. Galassi, R. D. Rivarola, Secondary electron emission from water vapor under 6.0 MeV/u $C^{6+}$ ion impact, Journal of Physics: Conference Series 388 (10) (2012) 102029.

[24] M. E. Rudd, R. D. DuBois, L. H. Toburen, C. A. Ratcliffe, T. V. Goffe, Cross sections for ionization of gases by 5-4000-keV protons and for electron capture by 5-150-keV protons, Physical Review A 28 (6) (1983) 3244–3257.

[25] M. A. Bernal, Evaluation of the mean energy deposit during the impact of charged particles on liquid water, Physics in Medicine and Biology 57 (7) (2012) 1745–1757.

[26] D. Belkić, Single charge exchange in collisions of energetic nuclei with biomolecules of interest to ion therapy, Zeitschrift für Medizinische Physik 31 (2) (2021) 122–144.

[27] D. Belkić, Review of theories on ionization in fast ion-atom collisions with prospects for applications to hadron therapy, Journal of Mathematical Chemistry 47 (4) (2010) 1366–1419.

[28] L. C. Tribedi, Ionization of large biomolecules by fast heavy ions, Vol. Volume 2, World Scientific, (2019), pp. 59–98.

[29] M. Inokuti, Inelastic collisions of fast charged particles with atoms and molecules—the bethe theory revisited, Reviews of Modern Physics 43 (3) (1971) 297–347.

[30] P. Hohenberg, W. Kohn, Inhomogeneous electron gas, Physical Review 136 (3B) (1964) B864–B871.

[31] W. Kohn, L. J. Sham, Self-consistent equations including exchange and correlation effects, Physical Review 140 (4A) (1965) A1133–A1138.

[32] M. Dingfelder, D. Hantke, M. Inokuti, Electron inelastic scattering cross sections in liquid water, Radiat. Phys. Chem. 53 (1998) 1–18.

[33] U. Werner, K. Beckord, J. Becker, H. O. Lutz, 3d imaging of the collision-induced coulomb fragmentation of water molecules, Physical Review Letters 74 (11) (1995) 1962–1975.

[34] F. Gobet, S. Eden, B. Coupier, J. Tabet, B. Farizon, M. Farizon, M. J. Gaillard, M. Carré, S. Ouaskit, T. D. Märk, P. Scheier, Ionization of water by (20˘150)-keV protons: Separation of direct-ionization and electron-capture processes, Phys. Rev. A 70 (6) (2004) 062716.

[35] F. Gobet, B. Farizon, M. Farizon, M. J. Gaillard, M. Carré, M. Lezius, P. Scheier, T. D. Märk, Total, partial, and electron-capture cross sections for ionization of water vapor by 20-150 keV protons, Phys. Rev. Lett. 86 (17) (2001) 3751–3754.

[36] H. Luna, A. L. F. de Barros, J. A. Wyer, S. W. J. Scully, J. Lecointre, P. M. Y. Garcia, G. M. Sigaud, A. C. F. Santos, V. Senthil, M. B. Shah, C. J. Latimer, E. C. Montenegro, Water-molecule dissociation by proton and hydrogen impact, Physical Review A 75 (4) (2007) 042711.

[37] L. H. Toburen, S. L. McLawhorn, R. A. McLawhorn, K. D. Carnes, M. Dingfeldera, J. L. Shinpaugha, Electron emission from amorphous solid water induced by passage of energetic protons and fluorine ions, Rad. Res. 174 (2010) 107–118.

[38] J. L. Shinpaugh, R. A. McLawhorn, S. L. McLawhorn, K. D. Carnes, M. Dingfelder, L. H. Toburen,

Low-energy electron emission from condensed targets induced by fast ions, Journal of Physics: Conference Series 388 (13) (2012) 132015.

[39] M. Michaud, A. Wen, L. Sanche, Cross sections for low-energy (1–100 eV) electron elastic and inelastic scattering in amorphous ice, Radiation Research 159 (1) (2003) 3–22.